Desalination and Water Treatment
www.deswater.com

doi: 10.5004/dwt.2023.29348

293 (2023) 224–242
May

Biosorption of methylene blue dye using banana floret: kinetic, equilibrium, thermodynamic and mass transfer studies

Clint Sutherland*, Beverly Chittoo, Vikash Laltoo

Project Management and Civil Infrastructure Systems, The University of Trinidad and Tobago, Trinidad and Tobago (WI), Tel.: +868 497 5744; Fax: +868 643 1617; email: clint.sutherland@utt.edu.tt (C. Sutherland), Tel.: +868 770 3004; email: beverly.chittoo@utt.edu.tt (B. Chittoo), Tel.: +868 728 9787; email: vikashlaltoo@yahoo.com (V. Laltoo)

Received 18 October 2022; Accepted 5 February 2023

ABSTRACT

Colour removal from effluents remains one of the most challenging requirements faced by industries due to the difficulty of degrading dyes which consequently escape conventional wastewater treatment processes and persist in the environment. This study aimed to assess and optimise the dye adsorption performance of banana floret, a novel biosorbent. Batch experiments were conducted to assess the effects of particle size, pH, agitation, temperature, initial concentration and sorbent dose. Kinetic and equilibrium data were modelled, and mass transfer studies were conducted to elucidate the mechanisms of biosorption. Equilibrium data were best simulated using the Sips and Langmuir isotherm models. At an optimum pH of 6.0, biosorbent dose of 1.0 mg·L^{-1} and temperature of 300 K, a maximum sorption capacity of 219 mg·g^{-1} was observed. The kinetic data were best represented by the pseudo-second-order model. The dominant transport mechanism was attributed to intraparticle diffusion, while the dominant attachment mechanism was physical sorption. The Taguchi method, in combination with analysis of variance, was used to determine the optimum levels of operational parameters for maximising the biosorption of methylene blue by banana floret. The parameter group which produced the highest biosorption capacity and percent removal was determined to be A3-B1-C3 (initial concentration = 200 mg·L^{-1}, biosorbent dose = 500 mg·L^{-1}, contact time = 60 min) and A1-B3-C3 (initial concentration = 50 mg·L^{-1}, biosorbent dose = 2000 mg·L^{-1}, contact time = 20 min), respectively. Among these parameters, the initial concentration had the most significant effect on the biosorption capacity, while sorbent dose was most significant on percent removal. A predictive model based on a quadratic equation which incorporates the factor interactions was successfully developed and validated.

Keywords: Adsorption; Banana floret; Methylene blue; Taguchi analysis; Kinetics; Equilibrium

1. Introduction

Water pollution by dyeing industries continues to be a subject of environmental concern due to the large volume of effluent disposed of in watercourses [1]. There are over 100,000 different dyes and pigments available commercially, and it is estimated that the worldwide production of dye is over 700,000 metric tonnes annually [2]. Up to 200,000 tonnes of this total world production is released into the environment in wastewater due to improper dye uptake during dyeing processes, as well as the degree of fixation on the substrate and other process inefficiencies [3]. According to Mittal [4], apart from industrial applications, the use of synthetic dye in the food industry has increased five-fold in the past 60 y. The author went on to explain that the increased use of artificial dyes stems from their lower manufacturing cost and their ability to make food look more appealing. The presence of these dyes in watercourses is of significant concern due to their toxicity to

* Corresponding author.

aquatic life, mutagenic and carcinogenic nature to humans and their potential to cause skin allergies, nausea, skin irritation, and breathing difficulties [5]. Additionally, the presence of dyes in watercourses decreases light penetration and photosynthetic activities, consequently resulting in oxygen deficiency, disruption of the aquatic environment and reduced downstream beneficial uses such as recreation, consumption and irrigation [3]. Environmental regulations oblige industries to eliminate colour from their dye-containing effluents before disposal into water bodies [6,7]. However, colour removal from effluents is one of the most challenging requirements faced by industries because dyes are not easily degraded and consequently escape conventional wastewater treatment processes and persist in the environment. Thus, research into the removal of dyes from water remains worthwhile.

The topic of dye removal has been extensively studied using various physical, chemical and biological treatment processes. Biological treatment processes are the most economically used processes; however, due to the low biodegradability of dyes, conventional biological processes are not very efficient for achieving satisfactory colour elimination from concentrated wastes [8]. Chemical treatment processes such as coagulation, ozonation, and chlorination are more efficient but are often expensive and result in the generation of concentrated sludge, the disposal of which is another topic of environmental concern [9]. Physical treatment methods such as membrane-filtration processes, for example, nanofiltration, reverse osmosis, and adsorption have been successfully tested and reported in the literature. However, adsorption has been found to be superior to other techniques for water reuse due to its low initial cost, flexibility, simplicity of design and ease of operation [10–13].

According to Mariyam et al. [14] adsorption has established itself as one of the most reliable technologies for the treatment of water. Further, without creating any intermediate products or fragmenting target molecules, the technique is capable of removing and recovering organic and inorganic compounds from their solutions. To date, adsorption researchers have identified and elucidated the notable operational parameters for various adsorbent/adsorbate interactions, viz. the removal of polycyclic aromatic hydrocarbons using biochar [15], rice husk activated carbon [16] and organo-zeolite [17]; the removal of heavy metals using chitosan grafted polyaniline-OMMT nanocomposite [18], peat moss [19], *Bacillus polymyxa* [20]; the removal of dyes using silver doped manganese oxide-carbon nanotube nanocomposite [21], ZnO–nanorods–activated carbon [22], and fly ash [23].

Dye adsorption using activated carbon has been successfully tested and reported as an advantageous technique due to its high efficiency, high capacity owing to its large surface area, and the ability for large-scale dye removal application and its potential for regeneration [24,25]. However, commercial activated carbon is expensive; therefore, several researchers have explored alternative adsorbents, including natural materials such as *Pistacia khinjuk* [24], *Elaeagnus* stone [26], oil palm wood [27], Paulownia flower [28], fungus [29] and Holm oak [30]. The use of agricultural waste such as wheat shells [31], rice husk [32], cotton fibre [33], guava seeds [34], wheat bran [35], banana stalk waste [36], banana peel [37], periwinkle shells [38], bagasse [39] and yellow passion fruit waste [40] has attracted much attention recently due to their low cost, nontoxicity, availability and abundance. Additionally, due to their low cost, after these materials have been expended, they can be discarded without expensive regeneration [24].

The development of predictive models can save time and improve efficiency in experimentation and enable the effectual upgrade to full-scale systems [41]. However, due to the non-linearity and diversity of biosorption systems, it is often difficult to develop predictive models based on traditional one-parameter at a time optimization [42]. According to Azizi et al. [43], statistical experimental design provides maximum, actual and more reliable information with experimental runs as fewer as possible. Genichi Taguchi, between the years 1950 to 1957, successfully implemented his industrial design-of-experiment. Early international adaptation of his technique began in 1981 by companies such as Bell, Ford and Xerox [44]. Today, the Taguchi experimental design method is one of the well-known, unique and powerful techniques for product or process quality improvement. It is widely used for analysis of experiments and in optimization problems [45]. The Taguchi method differs in several aspects from other experimental design techniques. The method strongly relies on the researcher's experience in choosing the right parameters and their levels; it uses orthogonal arrays to investigate the main and interaction effects of parameters. The researcher has to determine a target for their response variables, and the methods suggest the use of a loss function to understand the variation from the desired values [43].

In this study, methylene blue is used as a model cation dye to assess the performance of banana floret for dye removal. The diverse application of methylene blue extends beyond 130 y. Notable, its applications extend to the medical, textile and paper industries. It has been reported to cause eye burns and possibly permanent injury in humans and animals, breathing difficulties, nausea, mental confusion and methemoglobinemia [46]. Banana plant is known as the largest herbaceous flowering plant in the world [47]. The banana blossom is an agricultural by-product and is abundantly available in the Caribbean, India, Sri Lanka and South East Asian countries [47]. The use of banana floret for the biosorption of dyes has not been reported in the literature.

In this research, the authors aim to determine the efficiency of banana floret for the biosorption of methylene blue dye from solution. The transport and attachment mechanisms of biosorption are to be elucidated through batch kinetic, equilibrium, thermodynamic, and mass transfer studies. The Taguchi method, in combination with analysis of variance (ANOVA) is used to determine the optimised conditions for dye removal, which would enable process design and the eventual up-scaling of the process.

2. Materials and methods

2.1. Preparation of the biosorbent

Batch biosorption experiments were conducted using banana floret. The floret was first separated from hand-picked

banana flowers, washed in distilled water and dried at 378 K for 24 h. It was subsequently crushed and sieved into different particle sizes. The average particle size on a sieve was determined as the geometric mean of the diameter openings in two adjacent sieves in the stack. The geometric mean size (GMS) is expressed as (diameter of upper sieve × diameter of lower sieve)$^{0.5}$ [48].

2.2. Analytical methods

Methylene blue ($C_{16}H_{18}ClN_3S$), a cationic dye of molecular weight of 319.852 ± 0.022 g·mol^{-1} and purity of 98%, which corresponds to methylene blue hydrochloride with three groups of water, was used in this study (Fig. 1). Stock solutions of 1,000 mg·L^{-1} were prepared by dissolving 1 g in 1,000 mL of distilled water (prepared using a Thermo Scientific , Waltham, Massachusetts, United States still of pH approximately 7 and conductivity < 5 μS·cm^{-1}). The concentration of methylene blue was determined at a wavelength of 665 nm using an ultraviolet spectrophotometer (Shimadzu Recording Spectrophotometer UV-1800, Kyoto, Kyoto, Japan).

2.3. Biosorption studies

2.3.1. Kinetic studies

Laboratory-scale batch biosorption studies were carried out using the parallel method according to EPA OPPTS method 835.1230 [50]. Experiments were carried out in duplicate at room temperature (300 ± 20 K) in a batch reactor with a biosorbent mass of 1.0 g·L^{-1} and spiked with 50 mL of 100 mg·L^{-1} synthetic solution. Sorbent masses were accurate to ±0.001 g, and solution volumes were accurate to ±0.5 mL. For each time interval, identical reaction mixtures were prepared, agitated to maintain complete mixed conditions on a mechanical shaker and removed at predetermined intervals of time [51]. The biosorbent was then separated by mechanical straining, and the filtrate/supernatant was subsequently tested for residual methylene blue ions. In order to monitor and control any interference due to leaching during the test period, a blank was prepared, which comprised distilled water and banana floret. Solution pH was adjusted using appropriate solutions of HCl and NaOH and measured with a pH meter (Accumet Research AR10, Fisher Scientific , Hampton, New Hampshire, United States).

2.3.2. Equilibrium studies

The effect of initial methylene blue concentration was studied in duplicate by equilibrating 1.0 g·L^{-1} of biosorbent in synthetic methylene blue solution of varying concentrations (within the range of 50–400 mg·L^{-1} to ensure maximum sorption capacity was attained). The effect of sorbent dose was studied by using varying sorbent doses (0.5–3 g·L^{-1}) with methylene blue solution (100 mg·L^{-1}) at 298 ± 2 K. The effect of temperature on biosorption was examined by agitating reaction mixtures in a shaking water bath (Julabo SW23, Julabo GmbH, Seelbach, Germany) at temperatures varying from 298 ± 2 K to 328 ± 2 K.

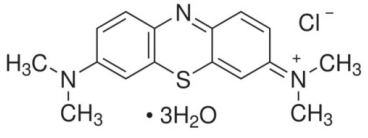

Fig. 1. Structure of methylene blue [49].

2.4. Kinetic models

Simulation of kinetic data was carried out using four models: Weber and Morris intraparticle diffusion model, Lagergren pseudo-first-order model, pseudo-second-order model, and the diffusion–chemisorption model.

2.4.1. Lagergren model

In 1898 Lagergren developed a first-order rate equation to describe the liquid–solid phase adsorption of oxalic acid and malonic acid onto charcoal. The model assumes a first-order rate based on surface reactions. To distinguish kinetic equations based on adsorption capacity from solution concentration, Lagergren's first-order rate equation has been called pseudo-first-order [52]. The non-linear and linear forms are:

$$q_t = q_e\left(1-\exp^{-K_{PFO}t}\right) \tag{1}$$

and

$$\log\left(q_e - q_t\right) = \log q_e - \frac{K_{PFO}}{2.303}t \tag{2}$$

2.4.2. Pseudo-second-order model

The pseudo-second-order equation was developed for the adsorption of divalent metal ions onto peat moss [53]. The model is based on pseudo-second-order chemical reaction kinetics [54] and is expressed in non-linear and linear forms as:

$$q_t = \frac{K_{PSO}q_e^2 t}{1+K_{PSO}q_e t} \tag{3}$$

and

$$\frac{t}{q_t} = \frac{1}{K_{PSO}q_e^2} + \frac{t}{q_e} \tag{4}$$

The initial sorption rate, h, as $t \to 0$ is expressed as:

$$h = \left(K_{PSO}\right)q_e^2 \tag{5}$$

2.4.3. Intraparticle diffusion model

Weber and Morris [55] proposed that the rate of intraparticle diffusion varies proportionally with the half power of time and is expressed as Eq. (6). If the rate-limiting step is intraparticle diffusion, a plot of solute adsorbed against the square root of time should yield a straight line passing through the origin [55].

$$q_t = K_{\mathrm{id}}\left(t^{1/2}\right) + c \tag{6}$$

2.4.4. Diffusion–chemisorption model

The diffusion–chemisorption kinetic model was developed to simulate the sorption of heavy metals onto heterogeneous media [56]. The model assumes that both diffusion and chemisorption are controlling mechanisms in the biosorption process. Non-linear and linear forms are as follows:

$$q_t = \frac{1}{\frac{1}{q_e} + \frac{1}{K_{\mathrm{DC}}} t^{0.5}} \tag{7}$$

and

$$\frac{t^{0.5}}{q_t} = \frac{t^{0.5}}{q_e} + \frac{1}{K_{\mathrm{DC}}} \tag{8}$$

Assuming a linear region as $t \to 0$, the initial rate is given as:

$$k_i = \frac{K_{\mathrm{DC}}^2}{q_e} \tag{9}$$

2.5. Mass transfer models

Mass transfer studies were conducted using the particle diffusion model, the intraparticle diffusion model, and the external film diffusion model.

2.5.1. External diffusion model

The external diffusion model assumes that during the initial stages of adsorption, intraparticle resistance is negligible, and transport is mainly due to film diffusion [57]. It was derived from an application of Fickian's law and expressed the concentration of solute in the solution as a function of the difference in concentration of the solute in the solution, C, and at the particle surface, C_i, in accordance with the following equation [58]:

$$\frac{dq}{dt} = -k_f S_0 \left(C - C_i\right) \tag{10}$$

Since C_i approaches zero and C approaches C_o, as $t \to 0$, Eq. (10) could be simplified [Eq. (11)] and k_f can be determined from the slope of the curve $\ln(C/C_o)$ vs. t:

$$\left[\frac{d\left(C/C_0\right)}{dt}\right]_{t=0} = -k_f S_0 \tag{11}$$

Assuming spherical particles, the surface area for mass transfer, S_o, can be obtained by the following equation [59]:

$$S_0 = \frac{6 m_S}{d_p \rho \left(1 - \varepsilon_p\right)} \tag{12}$$

2.5.2. Particle diffusion model

The model assumes that particle diffusion is rate-controlling and that Vermeulen's [60] approximation for particle diffusion [Eq. (13)] could be simplified to cover most of the data points for calculating effective particle diffusivity as follows:

$$X\left(t\right) = 1 - \frac{6}{\pi^2} \sum_{Z=1}^{\infty} \frac{1}{Z^2} \exp\left[\frac{-Z^2 \pi^2 D_e t}{r^2}\right] \tag{13}$$

where $X(t)$ is the fractional attainment at time t, given by:

$$X\left(t\right) = \frac{q_t}{q_e} \tag{14}$$

Vermeulen's [60] approximation of Eq. (13) is given as:

$$X\left(t\right) = \left[1 - \exp\left[-\frac{\pi^2 D_e t}{r^2}\right]\right]^{\frac{1}{2}} \tag{15}$$

A linear plot of $\ln[1/1 - X^2(t)]$ vs. t enables D_e to be calculated [61]:

$$\ln\left[\frac{1}{1 - X^2\left(t\right)}\right] = \frac{\pi^2}{r^2} D_e t \tag{16}$$

2.5.3. Biot number

The Biot number is a representation of the ratio of the rate of diffusion across the liquid film to the rate of diffusion within the particle and is determined using the following expression [62]:

$$B_i = \frac{k_f r}{D_e} \tag{17}$$

where k_f is the film diffusion coefficient, r is the particle radius, and D_e is the particle diffusion coefficient.

2.6. Isotherm models

The equilibrium capacity of banana floret for methylene blue was assessed by non-linear regression using two and three-parameter equilibrium models viz. the Langmuir isotherm, the Freundlich isotherm, the Redlich–Peterson isotherm, and the Sips isotherm.

2.6.1. Langmuir isotherm

The Langmuir model [Eq. (18)] is a theoretical equilibrium isotherm originally developed to relate the amount of gas adsorbed on a surface to the pressure of the gas [63]. The model assumes that sorption sites on the sorbent possess an equal affinity for molecules and that each site is capable of adsorbing one molecule, thus forming a monolayer.

$$q_e = \frac{q_L K_L C_e}{1 + K_L C_e} \tag{18}$$

The characteristic features of the Langmuir isotherm may be described in terms of the separation factor, $R_{L'}$ a dimensionless constant given by Eq. (19) [64].

$$R_L = \frac{1}{\left(1 + K_L C_0\right)} \tag{19}$$

This separation factor can be used to describe further the nature of the adsorption process. The isotherm is unfavourable if $R_L > 1$; linear if $R_L = 1$; favourable if $0 < R_L < 1$ and irreversible if $R_L = 0$.

2.6.2. Freundlich isotherm

Swan and Urquhart [65] explained that the equation of the form $x = kc^{1/n}$ was first applied to adsorption of gases by De Saussure in 1814. The application of this equation was further extended to solutions by Boedecker in 1859 [65]. In 1906, Freundlich described the adsorption isotherm mathematically as a special case for non-ideal and reversible adsorption [66]. This equation is presented in non-linear and linear forms as:

$$q_e = K_F \left(C_e\right)^{1/n_F} \tag{20}$$

$$\log\left(q_e\right) = \log\left(K_F\right) + \frac{1}{n_F}\log\left(C_e\right) \tag{21}$$

2.6.3. Redlich–Peterson isotherm

The Redlich–Peterson isotherm [Eq. (22)] is a hybrid isotherm that incorporates the features of the Langmuir and Freundlich isotherms [67]:

$$q_e = \frac{K_{\mathrm{RP}} C_e}{1 + \alpha_{\mathrm{RP}} C_e^{g_{\mathrm{RP}}}} \tag{22}$$

2.6.4. Sips isotherm

The Sips isotherm [Eq. (23)] is also a combined form of the Langmuir and Freundlich isotherms [68]. The model was developed for predicting heterogeneous adsorption systems and bypassing the limitation of the rising adsorbate concentration associated with the Freundlich isotherm model [69].

$$q_e = \frac{q_S \left(\alpha_S C_e\right)^{n_S}}{1 + \left(\alpha_S C_e\right)^{n_S}} \tag{23}$$

2.7. Thermodynamic studies

Thermodynamic studies were conducted under batch equilibrium conditions at four different temperatures (300, 308, 318 and 328 K) and assessed using parameters such as standard Gibb's free energy change ($\Delta G°$), enthalpy change ($\Delta H°$) and entropy change ($\Delta S°$). $\Delta G°$ was calculated using the following equation [70]:

$$\Delta G^\circ = -RT \ln K_d \tag{24}$$

where K_d is the distribution coefficient under equilibrium conditions calculated from the relationship (q_e/C_e).

According to Eq. (25), $\Delta S°$ and $\Delta H°$ were determined from the slope and intercept of linear plots of $\Delta G°$ vs. temperature, T, respectively.

$$\Delta G^\circ = \Delta H^\circ - T\Delta S^\circ \tag{25}$$

Activation energy E_a and sticking probability S^* were estimated using the linear form of a modified Arrhenius-type equation related to surface coverage given as:

$$\ln\left(1 - \theta\right) = \ln S^* + \frac{E_a}{RT} \tag{26}$$

where θ is the surface coverage expressed as:

$$\theta = \left(\frac{1 - C_e}{C_0}\right) \tag{27}$$

where S^* and E_a were determined from plots of $\ln(1 - \theta)$ vs. $1/T$ [70].

2.8. Error analysis

The goodness of fit by the various models to the experimental data was evaluated using the coefficient of determination, R^2, the hybrid error function (HYBRID), the Marquardt's percent standard deviation (MPSD), and the relative percent error (RPE) presented in Table 1.

2.9. Experimental design and procedure

The Taguchi method was applied to optimise and determine the level of significance of various operational parameters involved in the biosorption of methylene blue by banana floret. Minitab® statistical software was used for the range analysis and the analysis of variance (ANOVA) of the data and then to determine the most important operational factors, which can maximize the percent removal and biosorption capacity. In this study, the optimum values of particle size, pH and agitation speed we first elucidated as GMS 0.15 mm, 7.5, and 350 rpm, respectively. These parameters were kept constant at their optimum values. At the same time, three levels of varying amounts of biosorbent dose (500; 1,000 and 2,000 mg·L^{-1}), initial dye concentration (50, 100 and 200 mg·L^{-1}), and time (20, 40 and 60 min) were established. Consequently, a standardized L_9 (3^3) orthogonal array was selected based on the Taguchi design methodology, which involved nine experiments in order to cover the influences of the three parameters in three levels.

Azizi et al. [43] explained that in the Taguchi method, the term 'signal' represents the desirable value (mean) for the output characteristic, and the term 'noise' represents the undesirable value (standard deviation, SD) for the output characteristic. Therefore, the S/N ratio is the ratio of the mean to the SD. Taguchi uses the S/N ratio to measure the quality characteristic deviating from the desired value. Typically, there are three options for S/N ratios. These are the larger-the-better, the smaller-the-better, and the nominal-the-better. Because this study sought to maximize the biosorptive ability of the banana floret, the larger-the-better option was selected. In this case, the value of the S/N ratio can be calculated as follows [44,71]:

$$\frac{S}{N} = -10\log\left[\frac{1}{n}\sum\frac{1}{y_i^2}\right] \tag{32}$$

The following equation was applied to calculate the theoretically optimal S/N ratio [56]:

$$\eta_{\text{opt}} = -m_t + \sum_{i=1}^{q}\left(\eta_i - m_t\right) \tag{33}$$

The confidence interval (CI) for the predicted S/N ratio was determined as follows [71,72]:

$$\text{CI} = \pm\left[\frac{F_\alpha\left(1, f_e\right)V_e}{n_{\text{eff}}}\right]^{0.5} \tag{34}$$

where $F\alpha(1, f_e)$ is the variance ratio at a confidence level of $(1-\alpha)$ against degree of freedom (DOF) 1 and f_e is the DOF of error term, V_e is the error variance and n_{eff} is calculated by:

Table 1
Error functions

Expression	Equation number
$\text{RPE\%} = \frac{1}{N}\sum_{i=1}^{N}\frac{\left[\left\lvert\left(q_{e_i}\right)_{\text{pred}} - \left(q_{e_i}\right)_{\text{exp}}\right\rvert\right]}{\left(q_{e_i}\right)_{\text{exp}}} \times 100$	(28)
$\text{MPSD} = 100\sqrt{\frac{1}{N-P}\sum_{i=1}\left[\frac{\left(q_{e_i}\right)_{\text{exp}} - \left(q_{e_i}\right)_{\text{pred}}}{\left(q_{e_i}\right)_{\text{exp}}}\right]^2}$	(29)
$\text{HYBRID} = \frac{100}{N-P}\sum_{i-1}^{N}\left[\frac{\left(\left(q_{e_i}\right)_{\text{exp}} - \left(q_{e_i}\right)_{\text{pred}}\right)^2}{\left(q_{e_i}\right)_{\text{pred}}}\right]$	(30)
$R^2 = \frac{\sum_{i=1}^{N}\left(\left(q_{e_i}\right)_{\text{exp}} - q_{e_{\text{exp,mean}}}\right)^2 - \sum_{i=1}^{N}\left(\left(q_{e_i}\right)_{\text{exp}} - \left(q_{e_i}\right)_{\text{pred}}\right)^2}{\sum_{i=1}^{N}\left(\left(q_{e_i}\right)_{\text{exp}} - \left(q_{e_i}\right)_{\text{pred}}\right)^2}$	(31)

$$n_{\text{eff}} = \frac{N}{1 + \text{DOF}_{\text{opt}}} \tag{35}$$

where N is the total number of results, DOF_{opt} is the total degrees of freedom that are associated with the items used to estimate the value of η_{opt}.

3. Results and discussion

3.1. Kinetic modelling

3.1.1. Modelling the effects of agitation

Non-linear regression was performed using the Levenberg–Marquardt algorithm (Curve Expert Software©) to simulate primary biosorption data. The goodness of fit of each model to the experimental data was assessed using error functions presented in Table 1, which revealed that the pseudo-second-order model and diffusion chemisorption model produced the best simulations. Close examination of these results presented in Table 2 reveals the pseudo-second-order model produced the highest R^2 and the lowest MPSD, RPE, and HYBRID values in most instances. Consequently, the pseudo-second-order model was used to assess the kinetic manner of variations in mixing speed, pH and particle size on the biosorption process.

3.1.2. Effect of reaction time and mixing speed on biosorption

Fig. 2 shows the effect of agitation on the removal of methylene blue by banana floret. The figure reveals as agitation increased, the time to reach equilibrium decreased. At an agitation of 350 rpm, a high initial rate of removal is observed within the first 20 min (73% removal). Thereafter, the removal efficiency gradually climbed to 80% after 40 min. Finally, there was a marginal increase between 40 to 60 min of 3% as the reaction approached equilibrium. On the basis of these results, 60 min was selected as the time of equilibrium for further studies. Table 3 presents the pseudo-second-order model parameters obtained as a function

Table 2
Analysis of kinetic models using non-linear regression

rpm	Model	Linear regression			
		R^2	RPE	MPSD	HYBRID
150	Pseudo-first-order	0.951	13.09	23.98	88.6309
	Pseudo-second-order	0.986	8.78	17.59	41.1044
	Diffusion–chemisorption	0.985	9.29	21.19	51.4021
	Intraparticle diffusion	0.939	9.64	13.08	62.8876
250	Pseudo-first-order	0.951	12.67	26.72	121.71
	Pseudo-second-order	0.981	8.26	20.60	66.2364
	Diffusion–chemisorption	0.980	6.45	11.22	28.96
	Intraparticle diffusion	0.852	12.23	16.36	133.144
350	Pseudo-first-order	0.948	10.85	23.84	127.273
	Pseudo-second-order	0.983	6.59	14.48	45.7701
	Diffusion–chemisorption	0.963	8.54	14.48	58.8
	Intraparticle diffusion	0.677	17.38	23.46	331.129

of changing agitation speed. An increase in agitation speed resulted in increases in the biosorption capacity, initial, and overall reaction rate. This was expected as agitation promotes contact between media and liquid and maintains a high ion concentration gradient between the inner and outer regions of the particle [73]. Kuśmierek & Świątkowski [74] and Geethakarthi & Phanikumar [75], that an increase in agitation results in a reduction of the solvent film thickness, which surrounds the particle, and by extension, the resistance to film diffusion.

3.1.3. Effect of particle size on biosorption

The effect of particle size was studied with particle GMS varying from 0.15 to 0.65, at a constant pH, biosorbent dose and initial concentration of 6.0, 1.0 g·L^{-1} and 100 mg·L^{-1}, respectively. The results of pseudo-second-order modelling of the experimental data are presented in Table 3. It is observed that as particle size decreased, both the overall rate and the initial rate increased. According to Sutherland and Venkobachar [56], the reduction in particle size is accompanied by an increase in surface area, which can account for this increase in rate. Further, if the characteristics of the active sites on the surface of the banana floret are the same as those within the pores, then this increase in overall rate with decreased particle size is expected.

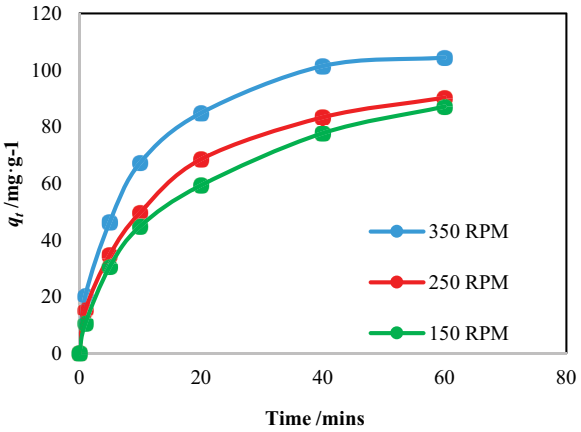

Fig. 2. Effect of mixing speed on methylene blue uptake.

Table 3
Pseudo-second-order model parameters for different operational parameters

Operational parameter	Values	K_{PSO} (g·mg^{-1}·min^{-1})	Initial rate (mg·g^{-1}·min^{-1})	q_e (mg·g^{-1})
pH	3	0.0014	4.1841	55.5556
	5	0.0012	15.0150	112.3596
	6	0.0013	17.7620	116.2791
	7.5	0.0015	18.3486	111.1111
	10	0.0014	16.9205	111.1111
Agitation (rpm)	150	0.0007	7.5451	103.8206
	250	0.0009	9.8282	104.5000
	350	0.0012	16.5315	117.3723
Particle GMS (mm)	0.17	0.0011	15.1539	104.4004
	0.35	0.0011	13.1812	96.1571
	0.6	0.0007	8.0992	80.7547

3.1.4. Effect of pH on biosorption

According to Elwakeel et al. [76], the pH of the dye solution is one of the most important parameters in controlling the sorption of the sorbate onto the sorbent. The effect of pH was studied using particle GMS of 0.35 mm, initial concentration of 100 mg·L^{-1} and agitation of 350 rpm and is presented in Fig. 3. Removal efficiency increased rapidly with an increase in pH, and reached a maximum of 90% at a value of pH 6. An increase in pH beyond 6 resulted in a marginal change in removal. According to Basker et al. [49], lower adsorption of methylene blue at acidic pH might be due to the presence of excess H^+ ions competing with dye cations for the available adsorption sites. However, in the basic medium, the formation of an electric double layer changes its polarity and consequently increases the methylene blue uptake [77]. Similar explanations were put forward by Guo et al. [78] and Hameed and El-Khaiary [79].

3.2. Equilibrium modelling

3.2.1. Modelling the effects of temperature

Further to presenting an overview of the path taken by the sorption system, adsorption isotherms reveal valuable insight into the efficiency of the sorbent in terms of its maximum sorption capacity and thus allow an estimate of the economic feasibility of the sorbent's commercial application for the specified solute [80]. Specifically, they aid in the development of predictive models enabling process design; determine whether a biosorbent can attain a particular treatment limit; provide a basis for comparison among various biosorbents; and aid in estimating the performance of full-scale batch and column systems [81]. Therefore, it cannot be overemphasized the importance of challenging the experimental data against various models to obtain an accurate simulation [73].

Simulation of the experimental data using two and three-parameter isotherm models was performed using

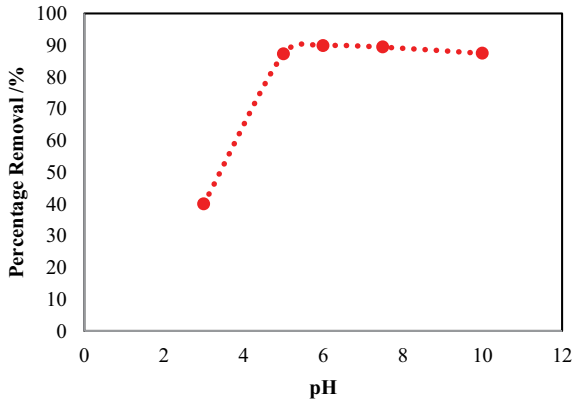

Fig. 3. Effect of pH on methylene blue uptake.

non-linear regression. The goodness of fit by each model was assessed using error functions presented in Table 1. Table 4 presents the results of analysis for the isotherm at particle GMS of 0.15 mm, pH at 6, agitation at 350 rpm, reaction time of 60 min and temperature ranging from 300 to 328 K. The Langmuir and Sips models produced the best simulation of the experimental data with a very marginal difference in precision in favour of the Sips model. Thus, in this study, the Sips equation is more appropriate for the development of predictive models. The significant correlation of the Langmuir model to the experimental data is sufficient to permit mechanistic inferences. The Langmuir isotherm is based on the assumption that points of valency exist on the surface of the sorbent and that each of these sites is capable of adsorbing one molecule [82]. Consequently, the adsorbed layer will be one molecule thick [82]. In accordance with Langmuir's assumption, it is therefore suggested that all the sorption sites on the banana floret have equal affinities for methylene blue ions and that the presence of adsorbed methylene blue ions at one site will not affect the sorption of ions at an adjacent site.

The Langmuir constant K_L is related to the binding energy or sorption energy coefficient, where a high value of K_L indicates a high affinity [83]. From Table 4, it is observed that both monolayer saturation capacity (q_m) and the affinity of methylene blue ions for the banana floret generally increase with increasing temperature, implying that the process is endothermic and favourable at higher temperatures. At higher temperatures, the increased kinetic energy of the sorbate ions increases its collision onto sorption sites and thus, the probability of attachment of sorbate ions to sorption sites increases. Using the Langmuir's constant K_L and Eq. (19), the shape of the isotherm was further evaluated by the dimensionless constant separation factor (R_L). Fig. 4 presents a plot of R_L vs. C_o for varying reaction temperatures. In all instances, the value of R_L was between 0 and 1, indicating a favourable uptake of methylene blue ions by the banana floret and, by extension, confirming the applicability of banana floret for column application [73]. It was also observed that an increase in reaction temperature resulted in decreasing R_L values which further confirms that biosorption was more favourable at higher temperatures.

According to the Langmuir isotherm, banana floret exhibited a monolayer saturation capacity of 219 mg·g^{-1}. This was compared to that of other biosorbents reported in the literature and presented in Table 5. The table reveals that the banana floret used in this study compares well to sorbents previously reported, which further suggests its effectiveness as a biosorbent.

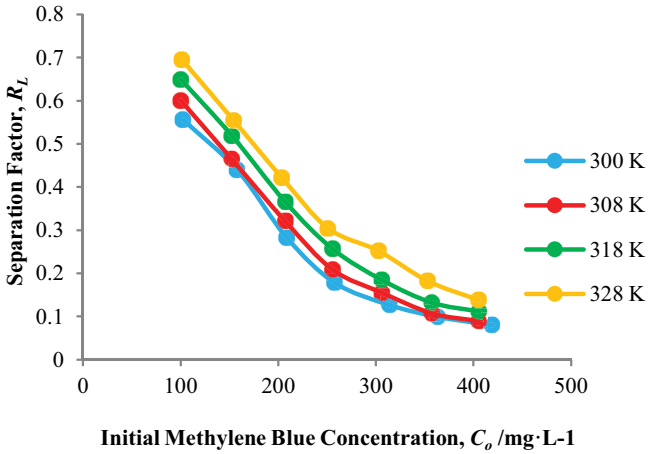

Fig. 4. Curves showing variation in separation factor for methylene blue biosorption using banana floret at different temperatures.

Table 4
Analysis of isotherm models using non-linear regression

Temperature (K)	Model	Constants			R^2	Error functions		
						RPE	MPSD	HYBRID
300	Langmuir	q_m = 219	K_L = 0.0545		0.9801	4.9113	7.5011	64.0294
	Freundlich	K_F = 56.9	n_F = 4.07		0.9452	7.9100	14.3820	208.1030
	Sips	α_S = 0.0576	q_S = 211	n_S = 1.16	0.9801	4.3101	6.5635	52.5236
	Redlich–Peterson	α_{RP} = 0.0602	K_{RP} = 12.4	g_{RP} = 0.988	0.9801	4.8924	7.7058	70.3141
308	Langmuir	q_m = 239	K_L = 0.0552		0.9880	3.8547	5.5084	36.8907
	Freundlich	K_F = 58.8	n_F = 3.84		0.9299	9.3588	15.6903	263.3338
	Sips	α_S = 0.0606	q_S = 224	n_S = 1.28	0.9920	2.2695	2.9294	14.6156
	Redlich–Peterson	α_{RP} = 0.0324	K_{RP} = 11.2	g_{RP} = 1.07	0.9920	16.8427	22.1972	919.8981
318	Langmuir	q_m = 266	K_L = 0.049		0.9920	2.3964	3.6835	18.5438
	Freundlich	K_F = 53.9	n_F = 3.33		0.9567	8.2615	13.8554	208.4577
	Sips	α_S = 0.0504	q_S = 262	n_S = 1.04	0.9920	2.1807	3.2422	15.4666
	Redlich–Peterson	α_{RP} = 0.052	K_{RP} = 13.2	g_{RP} = 0.992	0.9920	2.8629	3.8299	20.1833
328	Langmuir	q_m = 293	K_L = 0.0404		0.9920	2.2036	3.3678	22.8922
	Freundlich	K_F = 49	n_F = 2.97		0.9567	6.4779	12.0596	163.9632
	Sips	α_S = 0.0394	q_S = 297	n_S = 0.977	0.9920	2.1394	3.2988	22.0015
	Redlich–Peterson	α_{RP} = 0.0413	K_{RP} = 11.9	g_{RP} = 0.997	0.9920	2.3464	3.5320	25.6943

Table 5
Comparison of methylene blue dye biosorption capacity of various biosorbents reported in the literature

Biosorbent	Sorbent dose (g·L^{-1})	pH	Temperature (K)	Adsorption capacity, q_e (mg·g^{-1})	References
Rice husk	0.12	8	305	40.58	[32]
Pineapple stem waste	0.3	9	303	119.05	[84]
Bamboo	0.1	3.7	298	286.1	[85]
Dehydrated peanut hull	1.0	3.5	323	161.30	[86]
Wheat shells	1.0	6.5	323	21.50	[87]
Treated sawdust	0.2	7	298	263.16	[88]
Banana peel	0.2	–	–	120.0	[89]
Terminalia catappa shells	4.0	5	–	88.62	[90]
Penicillium glabrum (PG) fungi	0.33	8.2	303	16.67	[91]
Banana floret	0.5	6	300	219	This study

3.2.2. Effect of initial concentration

The effect of initial methylene blue concentration was studied at natural pH at room temperature using a constant biosorbent dose of 0.5 g·L^{-1}. Reaction mixtures were agitated at 350 rpm for 60 min. Fig. 5 shows the results as a function of both the percentage sorbed at equilibrium and the equilibrium sorption capacity. The figure reveals a gradual decrease in removal from 92% to 54% as initial sorbate concentration was increased from 50 to 400 mg·L^{-1}. At lower initial sorbate concentration, the ratio of sorption sites to total dye is high. Consequently, the dye ions could interact with the sorbent to occupy the sorption sites and be removed from the solution. However, at higher initial sorbate concentrations, the fixed number of sorption sites is insufficient to accommodate the large number of dye ions and thus, removal decreases [92]. The figure also reveals gradual increases in the mass of sorbate sorbed per unit weight of biosorbent with increasing sorbate concentration. Specifically, the sorption capacity of the banana floret increased from 47.25 to 221.04 mg·g^{-1} with an increase in initial concentration from 50 to 400 mg·L^{-1}. Banerjee and Chattopadhyaya [93] explained that higher sorbate concentrations result in steeper concentration gradients between the sorbent surface and the bulk solution. This increases the driving force necessary for overcoming mass transfer resistance between the solid and liquid phases. Hence the sorption capacity of the biosorbent is more completely utilized. Similar trends were reported by Omidi Khaniabadi et al. [94] for the removal of methylene blue from aqueous solution by activated carbon made from aloe vera waste and Jarusiripot [95] for the removal of reactive dye by chemically pretreated coal-based bottom ash.

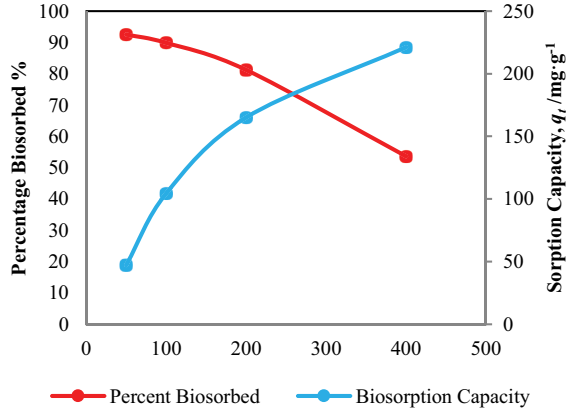

Fig. 5. Effect of initial methylene blue concentration.

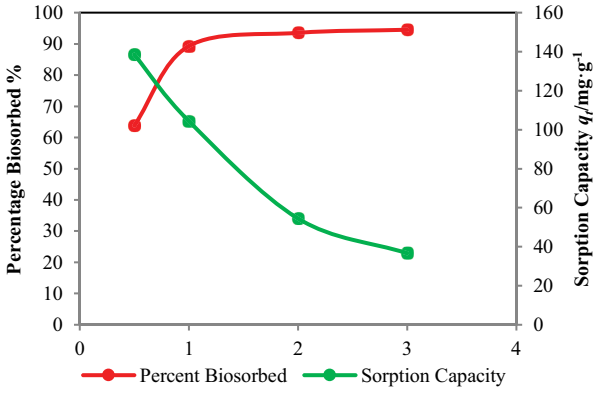

Fig. 6. Effect of biosorbent dose.

3.2.3. Effect of biosorbent dose

The effect of biosorbent dose was studied using a constant initial methylene blue concentration of 100 mg·L^{-1}. All reaction mixtures were agitated at 350 rpm for 60 min. Fig. 6 shows the effect of biosorbent dose as a function of both the percentage sorbed at equilibrium and the amount sorbed per unit weight of biosorbent. The figure reveals an increase in removal from 64% to 89% as the sorbent dose was increased from 0.5 to 1.0 g·L^{-1}. This increase in sorbed ions may be attributed to the increase in specific surface area and, thus, the availability of more sorption sites [96]. An increase in sorbent dose beyond 1 g·L^{-1} resulted in only a marginal increase in percent removal. According to Ozer et al. [97], this may have resulted due to the binding of almost all ions to the sorbent and the establishment of equilibrium between the ions bound to the sorbent and those remaining in solution. Namasivayam et al. [98], attributed this marginal increase in percent removal at higher sorbent

dosages to the overlapping of sorption sites as a result of overcrowding of sorbent particles. In spite of the significant increase in biosorbent dose and, thus, specific surface area, 100% removal was not achieved. This further implies that concentration gradient is a dominant driving force for biosorption onto banana floret. Thus, during batch treatment, greater process efficiency and economy can be accomplished by using multiple small batches rather than a single large batch [52].

Fig. 6 also reveals sharp decreases in the mass of sorbate sorbed per unit weight of biosorbent with increasing sorbent dose. At higher dosages, a more significant number of sorption sites are available for a finite number of sorbate ions resulting in non-saturation of more sorption sites per gram of sorbent at higher dosages. Thus, the biosorption capacity of the available biosorbent in the reaction mixture was not completely utilized at higher biosorbent dosages as opposed to lower biosorbent dosages [99]. Similar trends were reported by Shakoor and Nasar [100] for the utilization of *Punica granatum* peel as an eco-friendly biosorbent for the removal of methylene blue dye from aqueous solution and Chen et al. [101] for the adsorption of direct fast scarlet 4BS dye from aqueous solution onto natural superfine down particle.

3.2.4. Thermodynamic analysis

Equilibrium experiments conducted at varying temperatures showed increases in biosorption with increasing temperature implying that the process was endothermic in nature. The results of the thermodynamic analysis are presented in Table 6. For all temperatures and initial sorbate concentrations studied, $\Delta G°$ values were negative and decreased with an increase in temperature, indicating a spontaneous reaction in which more free energy was given off as temperature increased. In all instances, $\Delta G°$ was within the range 0 and –20 kJ·mol^{-1} and thus suggested that physisorption was involved in the biosorption process [102]. The positive values of $\Delta H°$ further confirm that the biosorption process was endothermic in nature. According to Saha and Chowdhury [103], the magnitude of $\Delta H°$ could be used to gain further insight into the mechanism of biosorption. The authors explained that $\Delta H°$ values within the range 2.1–20.9 kJ·mol^{-1} indicate physisorption, while values within the range 80–200 kJ·mol^{-1} indicate chemisorption. Nakajima and Sakaguchi [104] stated that $\Delta H°$ values less than 8.4 kJ·mol^{-1} indicates ion exchange reactions. Delle Site et al. as cited in [105] related the association $\Delta H°$ to the attachment mechanism as follows: direct and induced ion–dipole and dipole–dipole interactions (2–29 kJ·mol^{-1}); hydrophobic bonding (4 kJ·mol^{-1}); van der Waals interactions (4–8 kJ·mol^{-1}); charge transfer, ligand-exchange, and ion bonding (40 kJ·mol^{-1}); hydrogen bonding (2–40 kJ·mol^{-1}). In this work, it is found that $\Delta H°$ is a function of initial concentration. Further, $\Delta H°$ ranged from 4.906 to 20.302 kJ·mol^{-1}, implying that physisorption, ion exchange, van der Waals interactions, hydrogen bonding, and direct and induced ion–dipole and dipole–dipole interactions may be involved in the biosorption of methylene blue.

In all instances, $\Delta S°$ was positive due to increasing randomness at the solid/liquid interface during biosorption as the displaced water molecules gain more translational entropy than was lost by the sorbate ions or structural changes among the active sites of the biosorbent [106]. The values of activation energy, E_a decreased with increasing initial concentration and ranged from 61.9327 to 4.351 kJ·mol^{-1}. According to Chakravarty et al. [107], activation energy values between 5 and 40 kJ·mol^{-1}, infer physisorption is the predominant adsorption mechanism, while values between 40 and 800 kJ·mol^{-1} indicate chemisorption processes. Generally, the results obtained in this study suggest that the nature of the adsorption process was physisorption. For all concentrations tested, the values of the sticking probability were less than 1, which reveals that the process was favourable.

3.3. Process optimization using the Taguchi method

Optimisation of the interaction of initial concentration, sorbent dose and time was carried out using the Taguchi method. The biosorption capacity and percentage of methylene blue sorbed were determined by batch kinetic experiments for each combination of operational parameters. The corresponding S/N ratios were determined using Eq. (32) and are presented in Table 7. The average of the S/N data at each level of each parameter is presented in Table 8. The highest mean S/N for each parameter is highlighted in italics and represents the optimal level for that parameter. The relative importance among the varied parameters is represented by the difference between the maximum and minimum mean S/N value for each parameter (delta), and this rank

Table 6
Thermodynamic parameters

C_o	ΔH	ΔS	ΔG				E_a	S^*
(mg·L^{-1})	(kJ·mol^{-1})	(kJ·mol^{-1}·K^{-1})	300 K	308 K	318 K	328 K		
100	9.0569	0.0833	–15.8204	–16.7524	–17.5554	–18.1811	61.9327	0.0465
150	4.906	0.069	–15.7098	–16.3796	–17.1828	–17.6134	37.1228	0.0520
200	9.6477	0.0809	–14.4718	–15.4603	–16.1947	–16.7837	19.5845	0.0735
250	14.976	0.0943	–13.1495	–14.2229	–15.2213	–15.7943	11.2888	0.1016
300	20.302	0.1092	–12.3423	–13.5718	–14.348	–15.5222	8.00680	0.1186
350	17.876	0.0986	–11.769	–12.4747	–13.384	–14.5473	5.7737	0.1421
400	14.909	0.0876	–11.331	–12.097	–13.1199	–13.7432	4.3511	0.1656

Table 7
Biosorption capacity and percentage of dye sorbed and corresponding S/N ratio

Run no.	Parameters			Biosorption capacity		Percentage sorbed	
	A	*B*	*C*	Exp. q_t (mg·g^{-1})	S/N ratio	Percentage %	S/N ratio
1	1	1	1	62.700	35.945	61.471	35.773
2	1	2	2	44.900	33.045	88.039	38.894
3	1	3	3	23.740	27.510	93.098	39.379
4	2	1	2	133.530	42.512	57.556	35.202
5	2	2	3	102.000	40.172	87.931	38.883
6	2	3	1	49.700	33.927	85.690	38.659
7	3	1	3	204.600	46.218	50.394	34.048
8	3	2	1	124.000	41.868	61.084	35.719
9	3	3	2	66.100	36.404	65.123	36.275

Table 8
S/N ratio response table for percentage and amount of dye biosorbed

Mean S/N ratio (Δ*B*)					
Parameters	1	2	3	Delta	Rank
Biosorption capacity					
A: Initial concentration (mg·L^{-1})	32.17	38.87	41.5	9.33	1
B: Mass of biosorbent (mg·L^{-1})	41.56	38.36	32.61	8.94	2
C: Contact time (min)	37.25	37.32	37.97	0.72	3
Percent removal					
A: Initial concentration (mg·L^{-1})	38.02	37.58	35.35	2.67	2
B: Mass of biosorbent (mg·L^{-1})	35.01	37.83	38.1	3.1	1
C: Contact time (min)	36.72	36.79	37.44	0.72	3

is also presented in Table 8. The adsorption capacity exhibits the greatest dependency on initial concentration, while percent removal was most influenced by sorbent dose. The optimum combinations within the experimental range to attain the highest biosorption capacity and percent removal were found to be A3-B1-C3 and A1-B3-C3, respectively.

ANOVA was used to determine the individual interactions of all of the control factors in the test design. Statistical variables such as sum of the square (SS), the degree of freedom (DOF), the variance (*V*), *F*-ratio of the factor (*F*), *P*-value and percentage contribution (*P*) were established. The results presented in Table 9 reveal that for maximum biosorption capacity, initial concentration produced the highest variance and the largest percent contribution to the variance, while biosorbent dose produced the highest variance and the largest percent contribution to the variance when percent removal was maximised. The ANOVA results correlated well with the direct analysis of S/N ratio with regard to the relative significance of parameters.

The *F*-ratio was used to assess the statistical significance of the parameters. The confidence interval is generally set at 90% for significant and 95% for very significant levels [56].

Table 9
Analysis of variance of the S/N ratios for percentage and amount of dye biosorbed

Source of variation	Degree of freedom (DOF)	Sum of squares (SS)	Variance (V)	*F*-ratio (F)	*P*-value	Percent %
Biosorption capacity						
A: Initial concentration (mg·L^{-1})	2	138.891	69.445	492.560	0.002	52.733
B: Mass of biosorbent (mg·L^{-1})	2	123.268	61.634	437.160	0.002	46.802
C: Contact time /min	2	0.941	0.471	3.340	0.231	0.358
Error	2	0.282	0.141			0.107
Total	8	263.382	131.691			100.000
Percent removal						
A: Initial concentration (mg·L^{-1})	2	12.300	6.150	43.620	0.022	39.472
B: Mass of biosorbent (mg·L^{-1})	2	17.637	8.819	62.550	0.016	56.603
C: Contact time /min	2	0.941	0.471	3.340	0.231	3.020
Error	2	0.282	0.141			0.905
Total	8	31.160	15.580			100.000

Thus, the critical points of the *F*-ratios were obtained with *F*(5%, 2, 2) = 19.00 and *F*(10%, 2, 2) = 9.00. Using Table 9, the *F*-ratios of the three parameters and those of the critical points were compared. Initial concentration and biosorbent dose were the most significant parameters affecting the dye adsorptive capacities and percent removal since the *F*-ratios were higher than 19.00. The biosorption time, within the range tested, had no significant influence on the result of the experiment, with the F_C-ratios less than 9.00.

3.4. Development of predictive model

Linear regression analyses were first attempted using Minitab® statistical software to develop a model to predict the dependant variable (biosorption capacity or percent removal) as a function of the independent variables, viz. initial concentration (*A*), biosorbent dose (*B*) and contact time (*C*). The developed first-degree equations to predict biosorption capacity and percent removal are presented in Eqs. (36) and (37), respectively.

$$\text{Biosorption Capacity} = 59.6 + 0.554(A) - 0.056(B) + 0.783(C) \quad (36)$$

$$\%\text{Removal} = 65.3 + 0.150(A) - 0.015(B) + 0.193(C) \quad (37)$$

Fig. 7 shows the goodness of fit, which is assessed by calculating the coefficient of determination, R^2 to be 0.903 and 0.779 for adsorption capacity and percent removal, respectively. In an attempt to improve the prediction, quadratic equations covering the factor interactions were formulated and are given as Eqs. (38) and (39) for adsorption capacity and percent removal, respectively. The equations produced a correlation of determination, R^2 in both instances of 1.0 (Fig. 8). Thus, the model showed exceptional precision in predicting biosorption performance.

$$\begin{aligned}\text{Biosorption Capacity} = {} & 8.32788 + 1.71927(A) \\ & - 0.08678(B) + 1.26655(C) - 0.00315(A^2) \\ & + 3.23E-05(B^2) - 0.00028(AB) \\ & - 0.00154(AC) - 0.00051(BC)\end{aligned} \quad (38)$$

$$\begin{aligned}\%\text{Removal} = {} & 18.81450 + 0.05256(A) + 0.11745(B) \\ & - 0.51332(C) - 0.00107(A^2) - 3.82E-05(B^2) \\ & - 6.63E-05(AB) + 0.00397(AC) + 0.00015(BC)\end{aligned} \quad (39)$$

3.5. Taguchi prediction of optimum operational conditions

The parameter group which produces the highest biosorption capacity and percent removal was determined to be A3-B1-C3 and A1-B3-C3, respectively. The theoretically predicted optimum S/N ratios were subsequently calculated using Eq. (33) and found to be 46.007 and 39.598 dB. To test the accuracy of the optimization, the confidence interval was calculated using Eqs. (3) and (4) (for N = 9, DOF_{opt} = 6, f_e = 2, $F_{0.05}(1, 2)$ = 18.51, V = 0.141) and found to be CI = +/–1.425 dB (Table 10). The expected results of S/N ratio were subsequently transformed into values of biosorption capacities and percent removal using Eq. (32) and are also presented in Table 10. The optimum adsorption capacity and percent removal were both points within the orthogonal array. The experimental maximum biosorption capacity and percent removal were 204.6 mg·g^{-1} and 93.098%, respectively. From Table 10, it is observed that the values of maximum biosorption capacity and percent removal lie within the CI limit and as such, system optimization was achieved at a 0.05 significance level.

Confirmation tests were carried out at the optimum parameter combinations and using experimental data not included in the orthogonal array. A comparison of the prediction by the regression models and the Taguchi method is presented in Table 11. According to Kivak as cited in Cetin et al. [108], for reliable statistical analyses, error values must be smaller than 20%. The quadratic regression equation produced the lowest error within the accepted range. It is therefore surmised that the optimum combinations and predicted responses are valid.

3.6. Mechanisms

The transfer of ions from a liquid phase to a solid phase usually involves a transportation stage followed by an

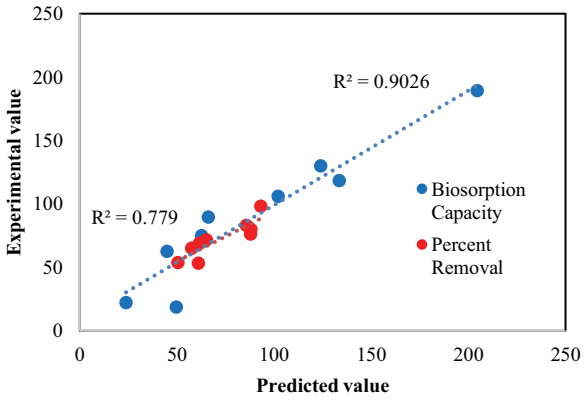

Fig. 7. Comparison of the linear regression model with experimental results.

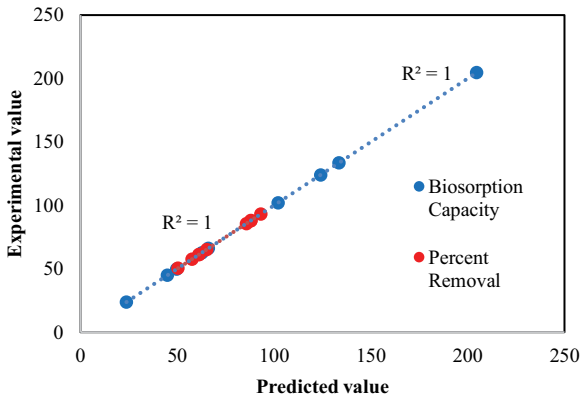

Fig. 8. Comparison of the quadratic regression model with experimental results.

Table 10
Taguchi prediction of peak adsorption capacity and percent removal

Dependant variable	Optimal combination	Predicted S/N ratio (dB)	Predicted parameter	CI of S/N ratio (dB)	Expected S/N ratio range (dB)	Expected parameter range
Biosorption capacity	A3-B1-C3	46.007	199.700 mg·g^{-1}	±1.425	44.582–47.437	169.473–235.424 mg·g^{-1}
Percent removal	A1-B3-C3	39.598	95.48%	±1.425	38.173–41.023	81.031%–112.499%

Table 11
Confirmation test results

Parameter group	Output parameter	Experimental value	Taguchi method		Linear regression equation		Quadratic regression equation	
			Predicted	Error (%)	Predicted	Error (%)	Predicted	Error (%)
A = 200 mg·g^{-1}; B = 500 mg;	q_t (mg·g^{-1})	204.600	199.700	2.395	189.380	7.439	204.600	0.000
C = 60 min (Optimum)	%	50.394	49.192	2.386	53.730	6.620	50.394	0.000
A = 50 mg·g^{-1}; B = 2,000 mg;	q_t (mg·g^{-1})	23.740	24.343	2.540	22.280	6.150	23.740	0.000
C = 60 min (Optimum)	%	93.098	95.476	2.554	98.280	5.566	93.097	0.001
A = 100 mg·g^{-1}; B = 500 mg;	q_t (mg·g^{-1})	114.000	135.190	18.588	102.000	10.526	116.000	1.754
C = 20 min (Random)	%	49.694	58.532	17.785	61.210	23.174	58.390	17.499
A = 100 mg·g^{-1}; B = 2,000 mg;	q_t (mg·g^{-1})	49.694	48.460	2.483	18.660	62.450	49.700	0.012
C = 20 min (Random)	%	85.670	83.540	2.486	82.960	3.163	85.689	0.022

attachment stage [109]. Thermodynamic analysis suggested that physisorption was the dominant attachment mechanism. Mass transfer studies were conducted to expound on the dominant transport mechanism.

3.6.1. Intraparticle diffusion model

The possibility of intraparticle diffusion was explored using the intraparticle diffusion model. The plots of q_t vs. $t^{1/2}$ (Fig. 9a–d) for varying agitation speed, particle size, initial dye concentration and sorbent dose exhibit multi-linearity. According to Fierro et al. [110], this implies that more than one rate-limiting step is involved in the biosorption process. The first sharper slope typically depicts the influence of external mass transfer, while the second slope is the gradual adsorption stage which is typically attributed to the influence of intraparticle diffusion.

3.6.2. External film diffusion model

The influence of film diffusion was assessed using the external film diffusion model. Table 12 reveals a progressive increase in k_f with an increase in agitation. This may be attributed to the decrease in external film resistance with increasing agitation, which influences the sorbate to reach the sorbent more rapidly [109]. The table also indicates that decreasing the GMS of the biosorbent resulted in a decrease in the external mass transfer coefficient. According to McKay et al. [111], this decrease in external mass transfer coefficient can be explained by the fact that for small particles, a large external surface area is presented to the sorbate molecules, which results in a lower driving force per unit surface area for mass transfer than when larger particles are used. A similar correlation is noted for variation in sorbent dose, where increasing the biosorbent dose resulted in a decrease in the external mass transfer coefficient. Conversely, it was observed that the mass transfer coefficient decreases with an increase in initial sorbate concentration. Similar results were obtained by McKay et al. [111] for the adsorption of phenol and p-chlorophenol onto activated carbon. The authors explained that while it is reasonable to expect that the increase in driving force with increasing initial concentration would increase the rate at which sorbate molecules pass from the bulk solution to the particle surface across the boundary layer, it is possible that increasing the concentration of sorbate, a larger and more polar species, reduces its mobility to transfer rapidly across the boundary layer. Despite the explainable trends, it was noted that in most instances, R^2 obtained when the external film diffusion model was fitted to the data was well below 0.95 and therefore implied that external mass transfer may not be rate-controlling.

3.6.3. Particle diffusion model

The impact of intraparticle diffusion was further assessed using the particle diffusion model. The results presented in Table 12 show an increase in D_e with increasing agitation. According to Ha et al. [112], as agitation increases, the diffusion barrier would decrease as particles move further apart, thereby increasing the diffusion coefficient. Table 12 also reveals an increase in the D_e values as sorbent dose increases. McKay et al. [113] explained that while it is expected that the mass transfer per unit surface area will decrease due to the increased surface area available with increasing mass, the mathematical dependence of this relationship is more complex since increasing the mass, changes the slope of the operating line on the sorption isotherm and also the terminal conditions of the dye

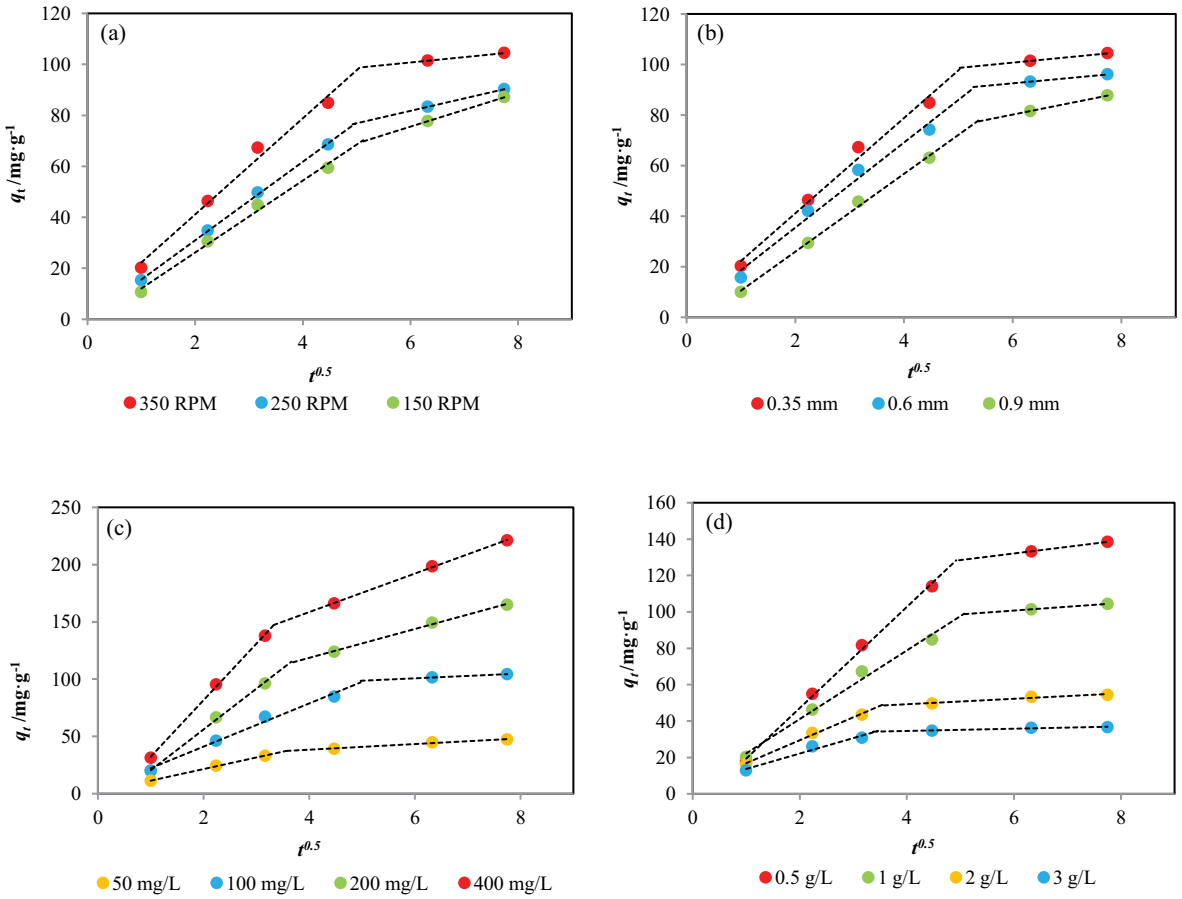

Fig. 9. Plots of the intraparticle diffusion model for varying (a) agitation, (b) particle size, (c) initial concentration and (d) sorbent dose.

in solution and the dye on the sorbent. According to Weber and Morris as cited in [113], the concentration dependence of a diffusion sorption process will vary depending on the characteristics of the sorption isotherm and on the fraction of solute sorbed at equilibrium. The authors further stated that only in instances where intraparticle diffusion was the sole rate-determining step was it found that D_e varied proportionally with the initial sorbate concentration. The results for varying initial dye concentrations in Table 12 reveal fluctuating values of D_e, which may indicate the combined effects of film and intraparticle diffusion. This complexity may have also led to the fluctuating trend in D_e values for varying particle size. Despite the shifting trends observed, it was noted that in all cases, coefficient of determination values was well above 0.96, indicating that while both film and intraparticle diffusion may be involved in the sorption process, intraparticle diffusion dominated.

3.6.4. Biot number

In order to confirm the dominance of intraparticle diffusion, the resulting mass transfer coefficients obtained from the external film diffusion and particle diffusion models were used to calculate the Bi number. According to Guibal et al. [114], Bi values < 100 indicate that external mass transfer dominates, while Bi > 100 indicates that intraparticle mass transfer dominates. The results presented in Table 12 are significantly higher than 100 and therefore confirm that the overall diffusion and sorption are mainly controlled by intraparticle diffusion.

3.7. Design of batch biosorption system from isotherm data

Laboratory-scale equilibrium studies are used to predict batch biosorber size and performance. It is assumed that a single-stage batch biosorber with a solution volume of V (L) and the initial methylene blue concentration, C_o is reduced to C_t as the reaction proceeds. The methylene blue loading on the biosorbent in the reactor of mass M (g) changes from q_0 to q_t with increased reaction time. Thus, the mass balance for the reactor is given by the following [115,116]:

$$V\left(C_0 - C_t\right) = M\left(q_t - q_0\right) = Mq_t \tag{40}$$

The biosorption process at 300 K was best represented by the Sips isotherm, thus the mass balance under equilibrium conditions ($C_t \to C_e$ and $q_t \to q_e$) is arranged as follows:

$$\frac{M}{V}\frac{C_0 - C_e}{q_e} = \frac{C_0 - C_e}{\dfrac{q_s\left(\alpha_s C_e\right)^{n_s}}{\left(1+\left(\alpha_s C_e\right)^{n_s}\right)}} \tag{41}$$

Table 12
Mass transfer coefficients and Bi for the biosorption of methylene blue

Operational parameter	Values	External diffusion model		Particle diffusion model		Bi
		R^2	k_f (cm·s^{-1})	R^2	D_e (cm^2·s^{-1})	
Agitation (rpm)	150	0.9754	0.000204	0.9892	2.5615E-09	676.9484
	250	0.9626	0.000255	0.9962	2.92742E-09	740.4123
	350	0.9185	0.000306	0.985	4.39113E-09	592.3298
GMS (mm)	0.17	0.9185	0.000306	0.985	4.39113E-09	592.3298
	0.35	0.9861	0.00525	0.9677	1.86129E-06	493.6082
	0.6	0.9581	0.0072	0.9818	4.10244E-06	526.5154
C_o (mg·L^{-1})	50	0.9438	0.000306	0.9984	3.65928E-09	710.7958
	100	0.9185	0.000306	0.985	4.39113E-09	592.3298
	200	0.9433	0.000204	0.9998	2.5615E-09	676.9484
	400	0.8694	0.000102	0.9964	2.5615E-09	338.4742
Sorbent dose (g·L^{-1})	0.0005	0.9203	0.000306	0.9939	4.02521E-09	646.178
	0.001	0.9185	0.000306	0.985	4.39113E-09	592.3298
	0.002	0.8635	0.000153	0.9939	4.75706E-09	273.383
	0.003	0.8003	0.000102	0.9878	5.48892E-09	157.9546

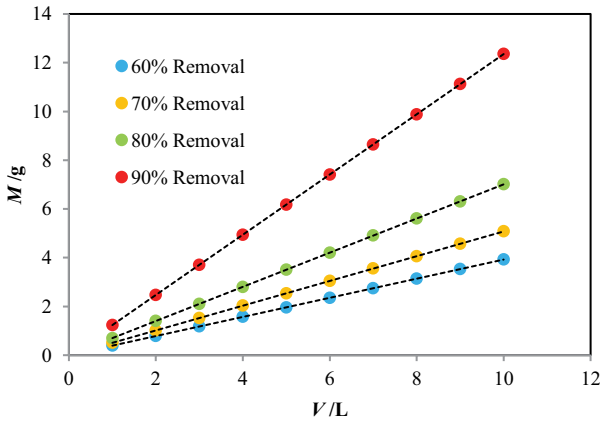

Fig. 10. Biosorbent mass (M) vs. volume of methylene blue solution treated (V).

Fig. 10 presents a series of plots of the predicted values of M (g) vs. V (L) for 60%, 70%, 80% and 90% methylene blue removal at the initial concentration of 100 mg·L^{-1} and 300 K. As an example, the biosorbent mass required for 90% methylene blue removal from aqueous solution was 6 and 11 g, for methylene blue solution volumes of 5 and 9 L, respectively. The preceding evaluation becomes relevant for pilot-batch system design as well as large-scale batch applications.

4. Conclusion

The objectives of this research were attained. The sorption performance of banana floret was assessed as a new biosorbent for methylene blue (a model cationic dye) removal. Banana floret exhibited a maximum sorption capacity of 219 mg·g^{-1} at a temperature of 300 K, which compared well to other sorbents reported in the literature. The optimum pH was found to be 6.0 and was observed to have a profound effect on the sorption process. Biosorption kinetic data were best simulated using the pseudo-second-order model while equilibrium data were best represented by the Sips and Langmuir isotherms. As particle size decreased, the initial and overall rate of the reaction increased. Mass transfer studies revealed that both film and intraparticle diffusion influenced the transport of methylene blue to biosorption sites; however, intraparticle diffusion dominated. Thermodynamic analysis suggested that physisorption was the most influential attachment mechanism. Application of the Taguchi method indicated that at optimum particle size, pH and agitation of GMS 0.15 mm, 6.0, and 350 rpm, respectively, the highest biosorption capacity could be obtained using an initial concentration = 200 mg·L^{-1}, biosorbent dose = 500 mg·L^{-1}, contact time = 60 min and the highest percent removal could be obtained using initial concentration = 50 mg·L^{-1}, biosorbent dose = 2,000 mg·L^{-1}, contact time = 20 min. Analysis by the Taguchi method revealed that sorption capacity exhibited the greatest dependency on initial concentration, while percent removal was most influenced by sorbent dose. A predictive model based on a quadratic equation which incorporates the factor interactions based on the Taguchi modelling, was successfully developed and validated.

Symbols

Bi — Biot number
C — Uniform concentration of the solute in the bulk of the liquid, mg·L^{-1}
C_e — Equilibrium concentration in solution, mg·L^{-1}
C_i — Concentration of the solute at the particle/liquid interface, mg·L^{-1}
C_o — Initial metal ion concentration, mg·L^{-1}
C_t — Concentration of metal ion at any time, mg·L^{-1}
d_p — Average particle diameter, cm
D_e — Particle diffusion coefficient, cm^2·min^{-1}

g_{RP} — Redlich–Peterson exponent
H — PSO initial rate, mg·g^{-1}·min^{-1}
k_i — DC initial rate, mg·g^{-1}·t^{-1}
k_f — Film mass transfer coefficient, cm·min^{-1}
K_{DC} — DC overall rate constant, mg·g^{-1}·t$^{-0.5}$
K_{id} — ID rate constant, mg·g^{-1}·t$^{-0.5}$
K_F — Freundlich constant related to adsorption affinity, mg·g^{-1}
K_L — Langmuir adsorption equilibrium constant, L·mg^{-1}
K_{PFO} — PFO rate constant, min^{-1}
K_{PSO} — PSO rate constant, g·mg^{-1}·min^{-1}
K_{RP} — Redlich–Peterson equilibrium constant
m_s — Mass of biosorbent particles per unit volume, g·cm^{-3}
M — Biosorbent mass, g
N — Number of replications for each experiment
n_F — Freundlich constant related to heterogeneity
N_s — Sips index of heterogeneity
η_{opt} — Predicted S/N ratio
m_t — Overall mean S/N ratio of all the efficiency values
η_i — Mean S/N ratio at the optimal level
N — Number of experimental points
P — Number of parameters in the regression model
Q — Adsorption efficiency
q_e — Equilibrium adsorption capacity, mg·g^{-1}
q_L — Langmuir monolayer sorption capacity, mg·g^{-1}
q_m — Maximum sorption capacity, mg·g^{-1}
q_t — Adsorption capacity at any time, mg·g^{-1}
q_S — Sips sorption capacity, mg·g^{-1}
R — Universal gas constant, 8.314 J·K^{-1}·mol^{-1}
R_L — Separation factor
R — Particle radius, cm
S_o — Surface area for mass transfer, cm^{-1}
T — Reaction time, min
T — Absolute temperature in K
V — Volume, L
V_e — Error variance from ANOVA
S^* — Sticking probability
E_a — Activation energy
y_i — Response for a given factor level combination

Greek

α_{RP} — Redlich–Peterson constant
α_S — Sips affinity constant
ε_p — Biosorbent porosity
P — True biosorbent solid phase density, g·cm^{-3}
ΔG — Gibb's free energy change
ΔS — Entropy change
ΔH — Enthalpy change

References

[1] S. David Noel, M.R. Rajan, Impact of dyeing industry effluent on groundwater quality by water quality index and correlation analysis, J. Pollut. Eff. Control., 2 (2014) 1–4, doi: 10.4172/2375–4397.1000126.
[2] I. Qadir, R.C. Chhipa, Comparative studies of some physicochemical characteristics of raw water and effluents of textile industries of Sitapura, Jaipur, Int. J. Adv. Res., 3 (2015) 2444–2449.
[3] F.M. Drumond Chequer, G.A.R. de Oliveira, E.R. Anastacio Ferraz, J. Carvalho Cardoso, M.V. Boldrin Zanoni, D.P. de Oliveir, Textile dyes: dyeing process and environmental impact, M. Günay, Ed., Eco-friendly textile dyeing and finishing, InTechOpen, 2013.
[4] J. Mittal, Permissible synthetic food dyes in India, Resonance, 25 (2020) 567–577.
[5] D.S. Malik, C.K. Jain, A.K. Yadav, R. Kothari, V.V. Pathak, Removal of methylene blue dye in aqueous solution by agricultural waste, Int. Res. J. Eng. Technol., 3 (2016) 864–880.
[6] C.J. Ogugbue, T. Sawidis, Bioremediation and detoxification of synthetic wastewater containing triarylmethane dyes by *Aeromonas hydrophila* isolated from industrial effluent, Biotechnol. Res. Int., 2011 (2011) 967925, doi: 10.4061/2011/967925.
[7] C. O'Neill, F.R. Hawkes, D.L. Hawkes, N.D. Lourenço, H.M. Pinheiro, W. Delée, Colour in textile effluents - sources, measurement, discharge consents and simulation: a review, J. Chem. Technol. Biotechnol., 74 (1999) 1009–1018.
[8] H. Dargo, N. Gabbiye, A. Ayalew, Removal of methylene blue dye from textile wastewater using activated carbon prepared from rice husk, Int. J. Innovation Sci. Res., 9 (2014) 317–325.
[9] M.A. Rahman, S.M.R. Amin, A.M.S. Alam, Removal of methylene blue from wastewater using activated carbon prepared from rice husk, Dhaka Univ. J. Sci., 60 (2012) 185–189.
[10] C. Li, Y. Dong, D. Wu, L. Peng, H. Kong, Surfactant modified zeolite as adsorbent for removal of humic acid from water, Appl. Clay Sci., 52 (2011) 353–357.
[11] H.S. Ashoka, S.S. Inamdar, Adsorption removal of methyl red from aqueous solution with treated sugar bagasse and activated carbon, Global J. Environ. Sci. Res., 4 (2010) 175–182.
[12] W.T. Tsai, C.Y. Chang, M.C. Lin, S.F. Chien, H.F. Sun, M.F. Hsieh, Adsorption of acid dye onto activated carbons prepared from agricultural waste bagasse by $ZnCl_2$ activation, Chemosphere, 45 (2001) 51–58.
[13] N. Kannan, A. Vijayakumar, P. Subramaniam, Studies on the removal of red industrial dye using teak leaf, maize corn and babool tree bark carbons – a comparison, E-J. Chem., 7 (2010) 770–774.
[14] A. Mariyam, J. Mittal, F. Sakina, R.T. Baker, A.K. Sharma, A. Mittal, Efficient batch and fixed-bed sequestration of a basic dye using a novel variant of ordered mesoporous carbon as adsorbent, Arabian J. Chem., 14 (2021) 103186, doi: 10.1016/j.arabjc.2021.103186.
[15] H. Li, R. Qu, C. Li, W. Guo, X. Han, F. He, Y. Ma, B. Xing, Selective removal of polycyclic aromatic hydrocarbons (PAHs) from soil washing effluents using biochars produced at different pyrolytic temperatures, Bioresour. Technol., 163 (2014) 193–198.
[16] S.M. Yakout, A.A.M. Daifullah, S.A. El-Reefy, Adsorption of naphthalene, phenanthrene and pyrene from aqueous solution using low-cost activated carbon derived from agricultural wastes, Adsorpt. Sci. Technol., 31 (2013) 293–302.
[17] J. Lemić, M. Tomašević-Čanović, M. Adamović, D. Kovačević, S. Milićević, Competitive adsorption of polycyclic aromatic hydrocarbons on organo-zeolites, Microporous Mesoporous Mater., 105 (2007) 317–323.
[18] R. Ahmad, I. Hasan, A. Mittal, Adsorption of Cr(VI) and Cd(II) on chitosan grafted polyaniline-OMMT nanocomposite: isotherms, kinetics and thermodynamics studies, Desal. Water Treat., 58 (2017) 144–153.
[19] C. Sutherland, B.S. Chittoo, C. Venkobachar, Application of an artificial neural network-genetic algorithm methodology for modelling and optimisation of the improved biosorption of a chemically modified peat moss: kinetic studies, Desal. Water Treat., 84 (2017) 69–84.
[20] L. Philip, L. Iyengar, C. Venkobachar, Site of interaction of copper on *Bacillus polymyxa*, Water Air Soil Pollut., 119 (2000) 11–21.
[21] V. Kumar, P. Saharan, A.K. Sharma, A. Umar, I. Kaushal, A. Mittal, Y. Al-Hadeethi, B. Rashad, Silver doped manganese oxide-carbon nanotube nanocomposite for enhanced dye-sequestration: isotherm studies and RSM modelling approach, Ceram. Int., 46 (2020) 10309–10319.

[22] E.A. Dil, M. Ghaedi, A.M. Ghaedi, A. Asfaram, A. Goudarzi, S. Hajati, M. Soylak, S. Agarwal, V.K. Gupta, Modeling of quaternary dyes adsorption onto ZnO-NR-AC artificial neural network: analysis by derivative spectrophotometry, J. Ind. Eng. Chem., 34 (2016) 186–197.
[23] K.V. Kumar, V. Ramamurthi, S. Sivanesan, Modeling the mechanism involved during the sorption of methylene blue onto fly ash, J. Colloid Interface Sci., 284 (2005) 14–21.
[24] M. Ghaedi, A.M. Ghaedi, F. Abdi, M. Roosta, A. Vafaei, A. Asghari, Principal component analysis-adaptive neuro-fuzzy inference system modeling and genetic algorithm optimization of adsorption of methylene blue by activated carbon derived from *Pistacia khinjuk*, Ecotoxicol. Environ. Saf., 96 (2013) 110–117.
[25] S. Dutta, B. Gupta, S.K. Srivastava, A.K. Gupta, Recent advances on the removal of dyes from wastewater using various adsorbents: a critical review, Mater. Adv., 2 (2021) 4497–4531.
[26] Ü. Geçgel, O. Üner, G. Gökara, Y. Bayrak, Adsorption of cationic dyes on activated carbon obtained from waste *Elaeagnus* stone, Adsorpt. Sci. Technol., 34 (2016) 512–525.
[27] S. Karaca, A. Gürses, M. Açıkyıldız, M. Ejder (Korucu), Adsorption of cationic dye from aqueous solutions by activated carbon, Microporous Mesoporous Mater., 115 (2008) 376–382.
[28] J. Chang, Z. Gao, X. Wang, D. Wu, F. Xu, X. Wang, Y. Guo, K. Jiang, Activated porous carbon prepared from Paulownia flower for high performance supercapacitor electrodes, Electrochim. Acta, 157 (2015) 290–298.
[29] A. Hassan, H.N. Bhatti, M. Iqbal, A. Nazir, Kinetic and thermodynamic studies for evaluation of adsorption capacity of fungal dead biomass for direct dye, Z. Phys. Chem. (N F), 235 (2021) 1077–1097.
[30] U. Tezcan Un, F. Ates, N. Erginel, O. Ozcan, E. Oduncu, Adsorption of Disperse Orange 30 dye onto activated carbon derived from Holm Oak (*Quercus Ilex*) acorns: a 3^k factorial design and analysis, J. Environ. Manage., 155 (2015) 89–96.
[31] Y. Bulut, N. Gözübenli, H. Aydin, Equilibrium and kinetics studies for adsorption of Direct blue 71 from aqueous solution by wheat shells, J. Hazard. Mater., 144 (2007) 300–306.
[32] V. Vadivelan, K.V. Kumar, Equilibrium, kinetics, mechanism, and process design for the sorption of methylene blue onto rice husk, J. Colloid Interface Sci., 286 (2005) 90–100.
[33] F. Uddin, A.R. Khan, H. Tahir, U. Hameed, Adsorption of methylene blue from aqueous solution on the surface of wool fiber and cotton fiber, J. Appl. Sci. Environ. Manage., 9 (2005) 17287, doi: 10.4314/jasem.v9i2.17287.
[34] C.G. Joseph, A. Bono, D. Krishnaiah, K.O. Soon, Sorption studies of methylene blue dye in aqueous solution by optimised carbon prepared from guava seeds (*Psidium guajava* L.), Mater. Sci. (Medžiagotyra), 13 (2007) 83–87.
[35] O. Hamdaoui, M. Chiha, Removal of methylene blue from aqueous solutions by wheat bran, Acta Chim. Slov., 54 (2007) 407–418.
[36] B.H. Hameed, D.K. Mahmoud, A.L. Ahmad, Sorption equilibrium and kinetics of basic dye from aqueous solution using banana stalk waste, J. Hazard. Mater., 158 (2008) 499–506.
[37] S.K. Shukla, N.R.S. Al Mushaiqri, H.M. Al Subhi, K. Yoo, H. Al Sadeq, Low-cost activated carbon production from organic waste and its utilization for wastewater treatment, Appl. Water Sci., 10 (2020), doi: 10.1007/s13201-020-1145-z.
[38] O.S. Bello, I.A. Adeogun, J.C. Ajaelu, E.O. Fehintola, Adsorption of methylene blue onto activated carbon derived from periwinkle shells: kinetics and equilibrium studies, Chem. Ecol., 24 (2008) 285–295.
[39] U. Kamran, H.N. Bhatti, S. Noreen, M.A. Tahir, S.-J. Park, Chemically modified sugarcane bagasse-based biocomposites for efficient removal of Acid red 1 dye: kinetics, isotherms, thermodynamics, and desorption studies, Chemosphere, 291 (2022) 132796, doi: 10.1016/j.chemosphere.2021.132796.
[40] F.A. Pavan, E.C. Lima, S.L.P. Dias, A.C. Mazzocato, methylene blue biosorption from aqueous solutions by yellow passion fruit waste, J. Hazard. Mater., 150 (2008) 703–712.
[41] B. Das, N.K. Mondal, R. Bhaumik, P. Roy, K.C. Pal, C.R. Das, Removal of copper from aqueous solution using alluvial soil of Indian origin: equilibrium, kinetic and thermodynamic study, J. Mater. Environ. Sci., 4 (2013) 392–408.
[42] S. Saraf, V.K. Vaidya, Statistical optimization of biosorption of Reactive orange 13 by dead biomass of *Rhizopus arrhizus* NCIM 997 using response surface methodology, Int. J. Ind. Chem., 6 (2015) 93–104.
[43] S.N. Azizi, M. Abrishamkar, H. Kazemian, Using of Taguchi robust design method to optimize effective parameters of methylene blue adsorption on ZSM-5 zeolite, Asian J. Chem., 23 (2011) 100–104.
[44] G. Taguchi, A.J. Rafanelli, Taguchi on robust technology development: bringing quality engineering upstream, J. Electron. Packag., 116 (1994), doi: 10.1115/1.2905506.
[45] C.M. Rao, K. Venkatasubbaiah, Optimization of surface roughness in CNC turning using Taguchi method and ANOVA, Int. J. Adv. Sci. Technol., 93 (2016) 1–14.
[46] M. Rafatullah, O. Sulaiman, R. Hashim, A. Ahmad, Adsorption of methylene blue on low-cost adsorbents: a review, J. Hazard. Mater., 177 (2010) 70–80.
[47] D.C.P. Ambrose, V. Sumithra, K. Vijay, K. Vinodhini, Techniques to improve the shelf life of freshly harvested banana blossoms, Curr. Agric. Res. J., 6 (2018) 141–149.
[48] H. Pfost, V. Headley, Methods of Determining and Expressing Particle Size, Feed Manufacturing Technology, 1976, pp. 512–517.
[49] A. Basker, P.S. Syed Shabudeen, P. Vignesh Kumar, Evaluation of adsorption potential of the agricultural waste areca husk carbon for methylene blue, Int. J. ChemTech Res., 6 (2014) 1309–1324.
[50] U.S. Environmental Protection Agency (USEPA), Fate, Transport, and Transformation Test Guidelines, Adsorption/Desorption (Batch Equilibrium), Washington, DC, OPPTS 835.1230, 2008, pp. 20–39.
[51] W.J. Weber Jr., C.T. Miller, Modeling the sorption of hydrophobic contaminants by aquifer materials—I. Rates and equilibria, Water Res., 22 (1988) 457–464.
[52] Y.S. Ho, G. McKay, A comparison of chemisorption kinetic models applied to pollutant removal on various sorbents, Process Saf. Environ. Prot., 76 (1998a) 332–340.
[53] Y. Ho, G. Mckay, Sorption of dye from aqueous solution by peat, Chem. Eng. J., 70 (1998b) 115–124.
[54] Y.S. Ho, G. McKay, Pseudo-second-order model for sorption processes, Process Biochem., 34 (1999) 451–465.
[55] W.J. Weber Jr., J.C. Morris, Kinetics of adsorption on carbon from solution, J. Sanit. Eng. Div., 89 (1963) 31–59.
[56] C. Sutherland, C. Venkobachar, A diffusion–chemisorption kinetic model for simulating biosorption using forest macrofungus, *Fomes fasciatus*, Int. Res. J. Plant Sci., 1 (2010) 107–117.
[57] Z. Aksu, I.A. Isoglu, Use of agricultural waste sugar beet pulp for the removal of Gemazol turquoise blue-G reactive dye from aqueous solution, J. Hazard. Mater., 137 (2006) 418–430.
[58] M. Jansson-Charrier, E. Guibal, J. Roussy, B. Delanghe, P. Le Cloirec, Vanadium(IV) sorption by chitosan: kinetics and equilibrium, Water Res., 30 (1996) 465–475.
[59] T. Furusawa, J.M. Smith, Fluid-particle and intraparticle mass transport rates in slurries, Ind. Eng. Chem. Fundam., 12 (1973) 197–203.
[60] T. Vermeulen, Theory for irreversible and constant-pattern solid diffusion, Ind. Eng. Chem., 45 (1953) 1664–1670.
[61] C. Lao-Luque, M. Solé, X. Gamisans, C. Valderrama, A.D. Dorado, Characterization of chromium(III) removal from aqueous solutions by an immature coal (leonardite). Toward a better understanding of the phenomena involved, Clean Technol. Environ. Policy, 16 (2014) 127–136.
[62] L.K. Lima, B.T. Pelosi, M.G. Silva, M.G. Vieira, Lead and chromium biosorption by *Pistia stratiotes* biomass, Chem. Eng. Trans., 32 (2013) 1045–1050.
[63] I. Langmuir, The adsorption of gases on plane surfaces of glass, mica and platinum, J. Am. Chem. Soc., 40 (1918) 1361–1403.
[64] K.R. Hall, L.C. Eagleton, A. Acrivos, T. Vermeulen, Pore- and solid-diffusion kinetics in fixed-bed adsorption under constant-pattern conditions, Ind. Eng. Chem. Fundam., 5 (1966) 212–223.

[65] E. Swan, A.R. Urquhart, Adsorption equations, J. Phys. Chem., 31 (1927) 251–276.
[66] H.M.F. Freundlich, Over the adsorption in solution, J. Phys. Chem., 57 (1906) 1100–1107.
[67] O. Redlich, D.L. Peterson, A useful adsorption isotherm, J. Phys. Chem., 63 (1959) 1024, doi: 10.1021/j150576a611.
[68] R. Sips, On the structure of a catalyst surface, J. Chem. Phys., 16 (1948) 490–495.
[69] A. Günay, E. Arslankaya, I. Tosun, Lead removal from aqueous solution by natural and pretreated clinoptilolite: adsorption equilibrium and kinetics, J. Hazard. Mater., 146 (2007) 362–371.
[70] H. Nollet, M. Roels, P. Lutgen, P. Van der Meeren, W. Verstraete, Removal of PCBs from wastewater using fly ash, Chemosphere, 53 (2003) 655–665.
[71] Y. Cao, A. Pawlowski, J. Zhang, Preparation of activated carbons with enhanced adsorption of cationic and anionic dyes from Chinese hickory husk using the Taguchi method, Environ. Prot. Eng., 36 (2010) 69–86.
[72] G. Nagpal, A. Bhattacharya, N.B. Singh, Cu(II) ion removal from aqueous solution using different adsorbents, Desal. Water Treat., 57 (2016) 9789–9798.
[73] C. Sutherland, A. Marcano, B. Chittoo, Artificial neural network-genetic algorithm prediction of heavy metal removal using a novel plant-based biosorbent banana floret: kinetic, equilibrium, thermodynamics and desorption studies, M. Eyvaz, E. Yüksel, Eds., Desalination and Water Treatment, InTechOpen, 2018.
[74] K. Kuśmierek, A. Świątkowski, The influence of different agitation techniques on the adsorption kinetics of 4-chlorophenol on granular activated carbon, React. Kinet. Mech. Catal., 116 (2015) 261–271.
[75] A. Geethakarthi, B.R. Phanikumar, Adsorption of reactive dyes from aqueous solutions by tannery sludge developed activated carbon: kinetic and equilibrium studies, Int. J. Environ. Sci. Technol. (Tehran), 8 (2011) 561–570.
[76] K.Z. Elwakeel, A.M. Elgarahy, G.A. Elshoubaky, S.H. Mohammad, Microwave assist sorption of crystal violet and Congo red dyes onto amphoteric sorbent based on upcycled Sepia shells, J. Environ. Health Sci. Eng., 18 (2020) 35–50.
[77] X. Han, L. Chu, S. Liu, T. Chen, C. Ding, J. Yan, L. Cui, G. Quan, Removal of methylene blue from aqueous solution using porous biochar obtained by KOH activation of peanut shell biochar, Bioresources, 10 (2015), doi: 10.15376/biores.10.2.2836-2849.
[78] Y. Guo, S. Yang, K. Yu, J. Zhao, Z. Wang, H. Xu, The preparation and mechanism studies of rice husk based porous carbon, Mater. Chem. Phys., 74 (2002) 320–323.
[79] B.H. Hameed, M.I. El-Khaiary, Equilibrium, kinetics and mechanism of malachite green adsorption on activated carbon prepared from bamboo by K_2CO_3 activation and subsequent gasification with CO_2, J. Hazard. Mater., 157 (2008) 344–351.
[80] C. Ng, J.N. Losso, W.E. Marshall, R.M. Rao, Freundlich adsorption isotherms of agricultural by-product-based powdered activated carbons in a geosmin-water system, Bioresour. Technol., 85 (2002) 131–135.
[81] C. Sutherland, C. Venkobachar, Equilibrium modeling of Cu(II) biosorption onto untreated and treated forest macrofungus *Fomes fasciatus*, Int. J. Plant Animal Environ. Sci., 3 (2013) 193–203.
[82] R.H. Perry, D. Green, Perry's Chemical Engineer's Handbook, 7th ed., McGraw-Hill, International Editions, New York, New York, United States, 1999.
[83] S. Islam, K. Ishikawa, Utilization of Bakuhanseki for the removal of cationic dye from aqueous solutions, J. Food Agric. Environ., 8 (2010) 1352–1356.
[84] B.H. Hameed, R.R. Krishni, S.A. Sata, A novel agricultural waste adsorbent for the removal of cationic dye from aqueous solutions, J. Hazard. Mater., 162 (2009) 305–311.
[85] Q. Liu, T. Zheng, N. Li, P. Wang, G. Abulikemu, Applied surface science modification of bamboo-based activated carbon using microwave radiation and its effects on the adsorption of methylene blue, Appl. Surf. Sci., 256 (2010) 3309–3315.
[86] D. Ozer, G. Dursun, A. Ozer, Methylene blue adsorption from aqueous solution by dehydrated peanut hull, J. Hazard. Mater., 144 (2007) 171–179.
[87] Y. Bulut, H. Aydın, A kinetics and thermodynamics study of methylene blue adsorption on wheat shells, Desalination, 194 (2006) 259–267.
[88] O.S. Bello, O.M. Adelaide, M.A. Hammed, Kinetic and equilibrium studies of methylene blue removal from aqueous solution by adsorption on treated sawdust, Maced. J. Chem. Chem. Eng., 29 (2010) 77–85.
[89] M. Dahiru, Z.U. Zango, M.A. Haruna, Cationic dyes removal using low-cost banana peel biosorbent, Am. J. Mater. Sci., 8 (2018) 32–38.
[90] L. Hevira, Zilfa, Rahmayeni, J.O. Ighalo, H. Aziz, R. Zein, *Terminalia catappa* shell as low-cost biosorbent for the removal of methylene blue from aqueous solutions, J. Ind. Eng. Chem., 97 (2021) 188–199.
[91] H.D. Bouras, Z. Isik, E.B. Arikan, A.R. Yeddou, N. Bouras, A. Chergui, L. Favier, A. Amrane, N. Dizge, Biosorption characteristics of methylene blue dye by two fungal biomasses, Int. J. Environ. Stud., 78 (2021) 365–381.
[92] T. Teka, S. Enyew, Study on effect of different parameters on adsorption efficiency of low cost activated orange peels for the removal of methylene blue dye, Int. J. Innov. Sci. Res., 8 (2014) 106–111.
[93] S. Banerjee, M.C. Chattopadhyaya, Adsorption characteristics for the removal of a toxic dye, tartrazine from aqueous solutions by a low-cost agricultural by-product, Arabian J. Chem., 10 (2017) S1629–S1638.
[94] Y. Omidi Khaniabadi, H. Basiri, A. Jafari, S. Saeedi, G. Goudarzi, F. Taheri, M. Salehi Murkani, Removal of methylene blue from aqueous solution by activated carbon from aloe vera wastes, Jundishapur J. Health Sci., 10 (2016), doi: 10.17795/jjhs-38242.
[95] C. Jarusiripot, Removal of reactive dye by adsorption over chemical pretreatment coal based bottom ash, Procedia Chem., 9 (2014) 121–130.
[96] H. Gebretsadik, A. Gebrekidan, L. Demlie, Removal of heavy metals from aqueous solutions using *Eucalyptus Camaldulensis*: an alternate low-cost adsorbent, Cogent Chem., 6 (2020) 1720892, doi: 10.1080/23312009.2020.1720892.
[97] A. Ozer, D. Ozer, A. Ozer, The adsorption of copper(II) ions on to dehydrated wheat bran (DWB): determination of the equilibrium and thermodynamic parameters, Process Biochem., 39 (2004) 2183–2191.
[98] C. Namasivayam, D. Prabha, M. Kumutha, Removal of direct red and acid brilliant blue by adsorption on to banana pith, Bioresour. Technol., 64 (1998) 77–79.
[99] H.C. Man, W.H. Chin, M.R. Zadeh, M.R.M. Yusof, Adsorption potential of unmodified rice husk for boron removal, BioResources, 7 (2012) 3810–3822.
[100] S. Shakoor, A. Nasar, Utilization of *Punica granatum* peel as an eco-friendly biosorbent for the removal of methylene blue dye from aqueous solution, J. Appl. Biotechnol. Bioeng., 5 (2018), doi: 10.15406/jabb.2018.05.00145.
[101] F. Chen, L. Xiong, M. Cai, W. Xu, X. Liu, Adsorption of direct fast scarlet 4BS dye from aqueous solution onto natural superfine down particle, Fiber Polym., 16 (2015) 73–78.
[102] R. Kumar, J. Rashid, M.A. Barakat, Synthesis and characterization of a starch-AlOOH-FeS_2 nanocomposite for the adsorption of Congo red dye from aqueous solution, RSC Adv., 4 (2014) 38334–38340.
[103] P. Saha, S. Chowdhury, Insight into adsorption thermodynamics, M. Tadashi, Ed., Thermodynamics, InTechOpen, 2011.
[104] A. Nakajima, T. Sakaguchi, Uptake and recovery of gold by immobilized persimmon tannin, J. Chem. Technol. Biotechnol., 57 (1993) 321–326.
[105] A. Delle Site, Factors affecting sorption of organic compounds in natural sorbent/water systems and sorption coefficients for selected pollutants. A review, J. Phys. Chem. Ref. Data, 30 (2001) 187–439.
[106] T.S. Anirudhan, P.G. Radhakrishnan, Thermodynamics and kinetics of adsorption of Cu(II) from aqueous solutions onto

a new cation exchanger derived from tamarind fruit shell, J. Chem. Thermodyn., 40 (2008) 702–709.
[107] S. Chakravarty, A. Mohanty, T.N. Sudha, A.K. Upadhyay, J. Konar, J.K. Sircar, A. Madhukar, K.K. Gupta, Removal of Pb(II) ions from aqueous solution by adsorption using bael leaves (*Aegle marmelos*), J. Hazard. Mater., 173 (2010) 502–509.
[108] M.H. Cetin, B. Ozcelik, E. Kuram, E. Demirbas, Evaluation of vegetable based cutting fluids with extreme pressure and cutting parameters in turning of AISI 304L by Taguchi method, J. Cleaner Prod., 19 (2011) 2049–2056.
[109] B.S. Chittoo, C. Sutherland, Phosphate removal and recovery using lime-iron sludge: adsorption, desorption, fractal analysis, modeling and optimization using artificial neural network-genetic algorithm, Desal. Water Treat., 63 (2017) 227–240.
[110] V. Fierro, V. Torné-Fernández, D. Montané, A. Celzard, Adsorption of phenol onto activated carbons having different textural and surface properties, Microporous Mesoporous Mater., 111 (2008) 276–284.
[111] G. McKay, M.J. Bino, A. Altememi, External mass transfer during the adsorption of various pollutants onto activated carbon, Water Res., 20 (1986) 435–442.
[112] J. Ha, C.R. Engler, S.J. Lee, Determination of diffusion coefficients and diffusion characteristics for chlorferon and diethylthiophosphate in Ca-alginate gel beads, Biotechnol. Bioeng., 100 (2008) 698–706.
[113] G. McKay, M.S. Otterburn, J.A. Aga, Intraparticle diffusion process occurring during adsorption of dyestuffs, Water Air Soil Pollut., 36 (1987) 381–390.
[114] E. Guibal, C. Milot, J.M. Tobin, Metal-anion sorption by chitosan beads: equilibrium and kinetic studies, Ind. Eng. Chem. Res., 37 (1998) 1454–1463.
[115] I.M. El-Naggar, E.S. Zakaria, I.M. Ali, M. Khalil, M.F. El-Shahat, Kinetic modeling analysis for the removal of cesium ions from aqueous solutions using polyaniline titanotungstate, Arabian J. Chem. 5 (2012) 109–119, https://doi.org/10.1016/j.arabjc.2010.09.028.
[116] G.E. Boyd, A.W. Adamson, L.S. Myers Jr, The exchange adsorption of ions from aqueous solutions by organic zeolites. II. Kinetics1, J. Am. Chem. Soc. 69 (1947) 2836–2848, https://doi.org/10.1021/ja01203a066.